Coherent Interactions of Terahertz Strain Solitons and Electronic Two-Level Systems in Photoexcited Ruby

Otto L. Muskens,[1,*] Andrey V. Akimov,[1,2] and Jaap I. Dijkhuis[1]

[1]*Debye Institute, Department of Physics and Astronomy, University of Utrecht, P.O. Box 80 000, 3508 TA, Utrecht, The Netherlands*
[2]*Ioffe Physico-Technical Institute, St. Petersburg 194021, Russia*

We observe coherent interactions between an ultrashort, longitudinal acoustic soliton train and the 29-cm^{-1} electronic transition in photoexcited ruby. Propagation of the strain pulses over millimeter distance through an excited zone reveals striking behavior of the induced electronic population, which has been explained by impulsive excitation of the two-level systems, combined with the nonlinear properties of the solitons in the resonant medium. This opens up new possibilities for coherent manipulation of ultrashort acoustic pulses by local electronic centers.

Recent efforts to generate coherent, longitudinal strain wave packets at THz frequencies have focused on ultrafast excitation of quantum wells and multilayer structures [1–3]. Thermoelastic generation methods employing a metallic film have been well developed, but remain limited to several hundreds of GHz by the optical skin depth and nonequilibrium electron transport [4,5]. For a long time, investigations of these transducer-generated picosecond strain pulses have been conducted only in the low-amplitude regime and over micrometer propagation distances. However, extension to higher strain amplitudes and larger crystals has opened up an entirely new range of nonlinear phenomena in picosecond ultrasonics. The first observations of strain solitons were made by Hao *et al.* [6] and showed consistency with the Korteweg–de Vries (KdV) equation. Experiments at even larger strain amplitudes, attainable using high-power laser excitation, demonstrated breakup of the initial strain wave packet into a train of ultrashort solitons in sapphire [7], predicting strain amplitudes up to 0.4% and soliton widths less than 0.5 ps.

In this Letter, we prove directly the presence of 0.87-THz frequency components in these soliton trains by coupling them to the well-known $\overline{E}(^2E) - 2\overline{A}(^2E)$ electronic transition in optically excited ruby. This system, known as the ruby phonon spectrometer, has been used for many years to study nonequilibrium phonons and related transport phenomena [8–11]. The experiments in this Letter, however, are of a fundamentally different nature, as the incident strain field excites a macroscopic acoustic polarization in the electronic system, as in GHz acoustic paramagnetic resonance [12]. The *half-cycle* nature and very high amplitude of the acoustic field allow for the experimental study of an entirely new regime of coherent electron-phonon interactions.

The studied sample is a $10 \times 10 \times 15$-mm^3 ruby crystal with one of the a axes perpendicular to a 10×15-mm^2 surface, which is covered by a 1000-Å chromium transducer. High-amplitude, picosecond strain wave packets are generated thermoelastically by absorption in the transducer of mJ optical pulses from an amplified Ti:sapphire laser, operating at 800 nm (see Ref. [7]). The sample is mounted in an optical cryostat with superconducting magnet, and immersed in superfluid helium at a temperature of 1.5 K. At similar experimental conditions, we have observed, independently, the development of strain solitons in the ruby crystal, using the Brillouin-scattering method of Ref. [7].

The excited-state $\overline{E}(^2E) - 2\overline{A}(^2E)$ doublets in a Cr^{3+} ion form a two-level system (TLS) with an energy splitting equal to 29 cm^{-1}, or 0.87 THz. The metastable density of TLS N^* can be simply controlled by the optical pumping cycle. We use a focused 2-W argon-ion laser to excite a pencil A [cf. Figure 1(a)] of about 200 μm in diameter up to densities of $N^* \approx 3 \times 10^{18}$ cm^{-3}. The R_2 and R_1 luminescence intensities, emanating from the $2\overline{A}$ and $\overline{E}$ levels, respectively, allow for a direct monitoring of the ratio of electronic level populations of the TLS. We collect the luminescence perpendicular to the argon-ion laser beam path. The time evolution of the R_2- and R_1-emission lines, at 692.8 and 694.2 nm optical wavelengths, is monitored using a double monochromator equipped with a time-resolved photon counting setup with a time resolution of 3 ns. Further, a small magnetic field of $\sim$0.2 T is applied to lift the degeneracy of the Kramers doublets, enhancing the speed of the ruby detector by a factor of 4 [11].

Figure 1 shows a typical R_2 luminescence signal normalized to the R_1 intensity at 5 mm from the transducer, for two configurations: one in which the path of the strain pulses is placed exactly in line with the excited zone ($\bigcirc$, on-axis), and one at a transverse displacement of 1.5 mm (solid line, off-axis). The off-axis traces are ordinary heat pulse signals [10], with the 1:3 ratio for the longitudinal (LA) and transverse (TA) acoustic phonon contributions, and arrival times that are in good agreement with the values calculated for corresponding phonon polarizations (vertical arrows in Fig. 1) for propagation along the ruby
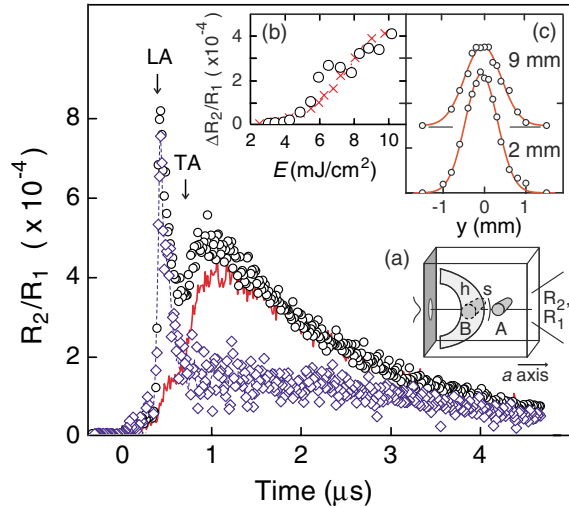
FIG. 1 (color online). Time-resolved R_2 luminescence normalized to R_1 at 5-mm propagation distance, for on-axis ($\bigcirc$) and off-axis (line/red) configurations, and in the presence of a secondary excited zone B ($\diamond$), at a pump fluence $E = 8.5$ mJ/cm^2. (a) Experimental configuration, with A and B excited volumes, s soliton pulse, and h heat pulse. (b) Soliton-induced LA intensity against pump fluence E at $z = 8$ mm and $N^* \approx 6 \times 10^{17}$ cm^{-3}, ($\bigcirc$) Experimental data, ($\times$) simulation results. (c) Transverse profiles of the soliton-induced LA intensity, at $z = 2$ mm and 9 mm, at $E = 8.5$ mJ/cm^2 pump fluence and $N^* \approx 6 \times 10^{17}$ cm^{-3}.

a axis. The on-axis signal exhibits a sharp spike at a time precisely corresponding to the travel time of the LA phonons from the transducer to the detection volume.

In order to clarify the nature of the on-axis LA peak, we point out three experimental observations. (i) The peak height shows a highly nonlinear dependence on the intensity of the ultrafast pump laser [see Fig. 1(b)]: The signal is absent at pump fluences below 4 mJ/cm^2, but rises quickly above 5 mJ/cm^2. (ii) The observed width of the transverse profile at 2-mm distance [see Fig. 1(c)] coincides with that of the pump laser at the position of the transducer, and only a slight broadening is observed after traversal over 9 mm, corresponding to a divergence angle of less than 0.5°. (iii) The directional component maintains its amplitude throughout the crystal, whereas the heat pulse decays strongly with distance, consistent with a hemispherical radiation source. Together with the independent Brillouin-scattering data, points (ii) and (iii) confirm that we are dealing with a soliton pulse which has frequency components at 0.87 THz. We show later that point (i) is also consistent with the soliton behavior.

To further explore the difference between the soliton and heat pulse signals, we changed the experimental configuration and included an additional excited zone B [cf. Figure 1(a)], in the path leading from the transducer to the detection zone A. For such a configuration, it is well known that both the ballistic LA and TA resonant phonons are strongly scattered by the excited Cr^{3+} ions in

zone B [10]. Indeed, we observe a reduction of the heat pulse TA contribution by about 70% of its value without zone B, as shown in Fig. 1. In contrast, the soliton-induced LA contribution remains unchanged, up to the highest $N^* \approx 3 \times 10^{18}$ cm^{-3} of zone B. Thus, the solitons are scattered by excited Cr^{3+} much less efficiently than conventional 29-cm^{-1} phonons in the heat pulse.

To investigate the scattering of the solitons by excited Cr^{3+} ions more precisely, we modified the configuration to the one shown in Fig. 2(a). The excited zone now consists of a ~0.6-mm wide cylinder *along* the path of propagation of the coherent acoustic beam. Luminescence is again detected at propagation distances z, imaging only a 0.2×0.5-mm^2 section of the center of the excited volume [zone A in Fig. 2(a)]. We again take the on- and off-axis difference to extract the soliton-induced signal. Figure 2 shows the amplitude of the soliton-induced signal as the obtained R_2/R_1 ratios against propagation distance z at three values of N^*. A gradual decrease as a function of propagation distance is observed, which resembles exponential decay (lines). We determine the mean-free path for solitons $\bar{l} = 7.0 \pm 1.0$ mm at the highest $N^* = 3 \times 10^{18}$ cm^{-3}. It is well known that the mean-free path $\bar{l}_r \approx 100$ nm for the resonant 29-cm^{-1} phonons at the same N^* [9–11,13]. This is 5 orders of magnitude less than the experimentally observed value for the soliton. Further, from the integral of the population ratios in Fig. 2 over the 1-cm long excited pencil, we calculate the energy converted from the wave packet to the electronic state to be ~1 μJ/cm^2. This is of the order of magnitude of the *total* energy of the strain wave packet, implying that significantly more is scattered from the solitons than just a near-resonant fraction.

In the following, we will interpret the key experimental features of the soliton-induced luminescence, namely, the insensitivity to an additional excited volume, its long mean-free path of several millimeters, and the threshold
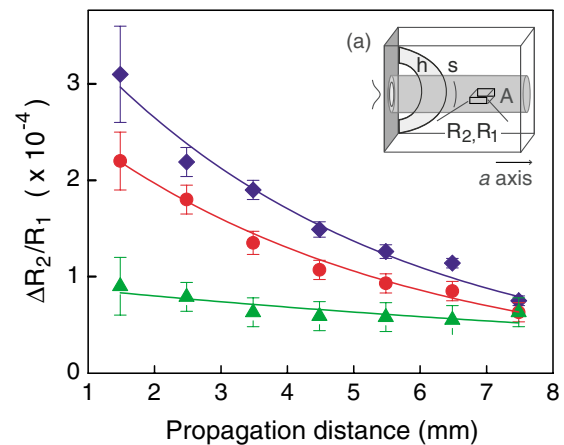
FIG. 2 (color online). Soliton-induced LA intensity as a function of propagation distance z for values of $N^* = 0.25$ ($\blacktriangle$), 0.8 ($\bullet$) and 2.5 ($\blacklozenge$) $\times 10^{18}$ cm^{-3}. (a) Experimental configuration, including detection volume A.

in the pump dependence. Linear response theory predicts the formation of a spectral hole in the propagating wave packet spectrum at the resonance frequency of the TLS, and would give the same behavior for the soliton as for the heat pulse. We will demonstrate below that the intrinsic nonlinearity of the strain solitons can fill in this spectral hole and efficiently funnel energy to the 29-cm^{-1} phonons via spontaneous emission.

The main property, responsible for the experimental observations, turns out to be the slightly higher velocity of the solitons than the velocity of sound [6,7]. We illustrate this statement using the simulations presented in Figs. 3(a) and 3(b). The interaction of a short pulse with the TLS results in the formation of trailing resonant strain radiation upon propagation [curve *1* in Fig. 3(a)] [14]. The presence of this radiation is responsible for the spectral hole for resonant modes in the combined spectrum of the strain wave after the interaction with TLS. The difference in velocities for soliton and conventional sound leads to a delay of the linear trailing radiation respective to the nonlinear soliton, proportional to the propagation distance z. A walk-off by 1/4 of a resonant phonon wavelength will occur within a distance of $l_s \approx 1.3$ μm for a typical 0.4% strain soliton [7]. This has far-reaching consequences for the development of the trailing radiation as can be seen in Fig. 3(a). In a dispersive medium with the resonant Beer's length $\bar{l}_r$, the trailing radiation disappears [curve *2* in Fig. 3(a)], which corresponds to a refilling of the spectral hole at the resonant modes in the frequency domain. Figure 3(b) shows the dependence of

the population of the resonant 0.87-THz modes in the strain packet which has traversed the resonant medium over a distance z. Curves *1* and *2* [Fig. 3(b)] correspond to the linear and nonlinear propagation regimes, respectively. The linear regime is accompanied with a strong attenuation of the resonant modes over $z \sim \bar{l}_r$, while in the nonlinear case the number of resonant modes is almost independent on z. As a result, the nonlinear regime allows one to convert almost all energy in the soliton to the energy of the resonant mode, which is emitted spontaneously by the TLS. Obviously, the linear regime cannot produce such a spectral redistribution.

Thus, the temporal and the spectral shape of the soliton wave packet do not change significantly with distance. This allows us to simplify the analysis and assume that each atom in the excited volume experiences exclusively impulsive excitation by the solitons. Analogue to optics, we consider the electronic system as a pendulum that may be excited either through a resonant driving field or by impulsive action. The latter regime is commonly ignored in optics as it requires pulses shorter than the resonant period of the electronic state. For a quantitative description, we make use of the original set of Bloch equations [15], which has been used earlier in the studies of few-cycle optical pulses [16]. In this model, no approximations are made that assume a slowly varying envelope on a fast carrier wave [12,15]. Rather, the strain waveform $s(t)$ acts directly on the "carrier" Rabi frequency $\chi(t)$ proportional to the matrix element χ_0 of the $\overline{E}(^2E) - 2\overline{A}(^2E)$ transition, estimated to a value of $\hbar\chi_0 \approx 200$ cm^{-1} per unit of uniaxial strain along the ruby a axis [17,18]. Subsequently, the phase of the electronic state vector rotates with resonance frequency ω_0 and decays by spontaneous emission, $T_1 \approx 0.7$ ns [13], and $T_2 = 2T_1$. For completeness, we give the full evolution equation for the electronic state vector $\mathbf{S}$:

$$\frac{\partial}{\partial t}\mathbf{S} = \boldsymbol{\beta} \times \mathbf{S} - \boldsymbol{\Gamma} \cdot (\mathbf{S} - \mathbf{S}_0), \tag{1}$$

with the usual conventions for relaxation $\boldsymbol{\Gamma}$, initial state $\mathbf{S}_0 = (0, 0, -1)$, and pseudofield vector $\boldsymbol{\beta} = (2\chi(t), 0, \omega_0)$.

Knowing the state vector $\mathbf{S}$, we can calculate the population ratio $\Delta w/2$ of the electronic levels by projection onto the vertical axis. Numerical simulations of $\Delta w/2$, during the passage of a realistic soliton train (see Ref. [7]), are shown in Fig. 3(c). It is observed that excitation of the two-level system is induced primarily by the first five pulses in the train, consisting of 11 solitons. In contrast to the sharp steps produced by these first solitons, which are the shortest and have the highest amplitude, excitation by the longer pulses at the end is suppressed by the precession of the state vector at its natural frequency ω_0. We also observe that, for the fourth and sixth solitons, we have a *decrease* in the population. This is similar to coherent control experiments, where the result of the short pulse excitation depends critically on the phase of the electronic state [19]. The obtained
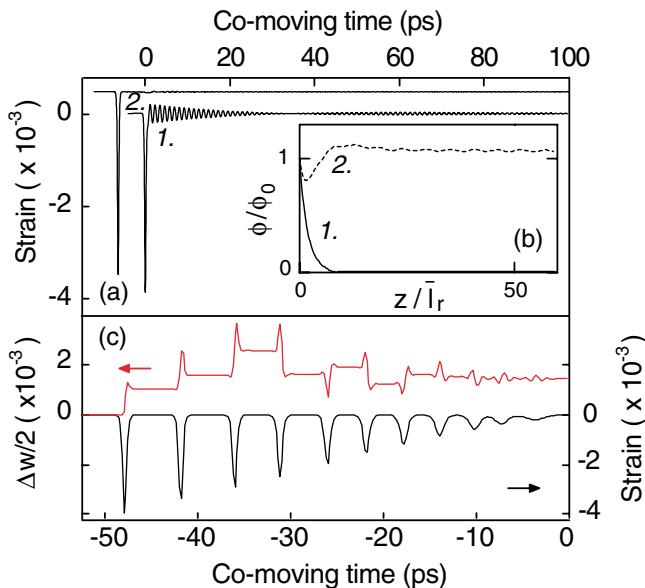
FIG. 3 (color online). (a) Time-domain profile of a 0.4% strain pulse after propagation over $150\bar{l}_r$ in a resonant medium, for *1* linear propagation, no walk-off, and *2* with soliton walk-off, $l_s = 13\bar{l}_r$. (b) Resonant Fourier component ϕ at 0.87 THz against traversed distance $z/\bar{l}_r$ for situations *1.* (solid line) and *2.* (dashed line). (c) Simulated population ratio $\Delta w/2$ (upper line/red) for a typical KdV soliton train [7] (lower line/black).

excitation $\Delta w/2 \approx 2 \times 10^{-3}$ corresponds to a Bloch angle of about $4°$, which means that the excitation remains well within the linear regime of the harmonic oscillator.

The measured R_2 to R_1 is of the order of magnitude of the calculated $\Delta w/2$ for the typical soliton train in Fig. 3(c). For more precise quantitative agreement between simulated and experimental R_2/R_1 ratios in Fig. 1(b), we correct for the bottleneck efficiency [9–11] and radiative probabilities of the R lines [20]. We have simulated the excited population for soliton trains at various initial strain amplitudes and plotted the results for R_2/R_1 in Fig. 1(b) ($\times$/solid line), where the horizontal scale was calibrated using the independent Brillouin-scattering data, similar to Ref. [7]. We obtain good agreement in both the offset at ~ 4 mJ/cm^2 and the steep increase of the signal at higher pump fluences.

Our estimate of $\Delta w/2$ of 2×10^{-3} adds up to a total energy of $\sim 1~\mu$J/cm^3 at $N^* = 10^{18}$ cm^{-3}, and thus to a soliton mean-free path of ~ 1 cm, in close agreement with the experiments of Fig. 2.

Experimental results are in excellent agreement with the presented model where the slight difference in velocities for soliton and the linear sound takes place. The mean-free path for the soliton pulse is much larger than for resonant phonons from the heat pulse. Further, the integral of the energy transferred from the soliton to the TLS medium at this distance is of the order of the total energy in the initial strain packet.

The presented work predicts new avenues for the manipulation of ultrashort acoustic pulses using local electronic centers. A challenging possibility is the amplification of coherent THz strain wave packets using inverted two-level systems, attainable by direct optical excitation of the $2\bar{A}(^2E)$ states. The transducer-generated ultrashort strain solitons may then serve as a trigger for starting up the coherent release of the acoustic polarization in the form of a resonant tail. In this situation, the area theorem [14,15] predicts exponential growth of the Bloch angle of this tail over the submicrometer, *resonant absorption length* $\bar{l}_r$, anticipating an exponential factor $L_c/\bar{l}_r \approx 200$, with $L_c = c_0 T_1$ the length over which the inversion can be maintained using pulsed optical excitation of the Cr^{3+} ions [21]. Amplification over several orders of magnitude and concomitant breakup of the wave packet into a new kind of THz strain solitons, the resonant 2π pulses of self-induced transparency, appears well within the range of possibilities.

In conclusion, we have observed coherent interaction between an acoustic soliton train and the $\bar{E}(^2E) - 2\bar{A}(^2E)$ electronic transition in photoexcited ruby, explicitly demonstrating the development of strain components in the solitons of frequencies as high as 0.87 THz. The soliton-induced signal was found to be highly directional, strongly dependent on pump fluence, and only weakly influenced by dissipation through the interaction with the electronic system. We have explained the key experimental observations using only simple arguments based on nonlinear refilling of the spectral hole and impulsive excitation of the two-level systems by the soliton train.

*Electronic address: O.L.Muskens@phys.uu.nl

[1] A. Bartels, T. Dekorsy, H. Kurz, and K. Köhler, Phys. Rev. Lett. **82**, 1044 (1999).

[2] Ü. Özgür, C.-W. Lee, and H. O. Everitt, Phys. Rev. Lett. **86**, 5604 (2001).

[3] A. Kent, N. M. Stanton, L. Challis, and M. Henini, Appl. Phys. Lett. **81**, 3497 (2002).

[4] C. Thomsen, H. T. Grahn, H. J. Maris, and J. Tauc, Phys. Rev. B **34**, 4129 (1986).

[5] O. B. Wright and K. Kawashima, Phys. Rev. Lett. **69**, 1668 (1992).

[6] H.-Y. Hao and H. J. Maris, Phys. Rev. B **64**, 064302 (2001).

[7] O. L. Muskens and J. I. Dijkhuis, Phys. Rev. Lett. **89**, 285504 (2002).

[8] K. F. Renk and J. Deisenhofer, Phys. Rev. Lett. **26**, 764 (1971).

[9] J. E. Rives and R. S. Meltzer, Phys. Rev. B **16**, 1808 (1977).

[10] A. A. Kaplyanskii and S. A. Basun, in *Nonequilibrium Phonons in Nonmetallic Crystals*, edited by W. Eisenmenger and A. A. Kaplyanskii (North-Holland, Amsterdam, 1986), p. 373.

[11] R. J. G. Goossens, J. I. Dijkhuis, and H. W. de Wijn, Phys. Rev. B **32**, 7065 (1985).

[12] N. S. Shiren, Phys. Rev. B **2**, 2471 (1970).

[13] M. H. F. Overwijk, P. J. Rump, J. I. Dijkhuis, and H. W. de Wijn, Phys. Rev. B **44**, 4157 (1991).

[14] D. C. Burnham and R. Y. Chiao, Phys. Rev. **188**, 667 (1969).

[15] L. Allen and J. H. Eberly, *Optical Resonance and Two-Level Atoms* (Dover, New York, 1987), 2nd ed.

[16] R. W. Ziolkowski, J. M. Arnold, and D. M. Gogny, Phys. Rev. A **52**, 3082 (1995).

[17] M. Blume, R. Orbach, A. Kiel, and S. Geschwind, Phys. Rev. **139**, 314 (1965).

[18] S. M. Sharma and Y. M. Gupta, Phys. Rev. B **43**, 879 (1991).

[19] N. Dudovich, D. Oron, and Y. Silberberg, Phys. Rev. Lett. **88**, 123004 (2002).

[20] S. Sugano and Y. Tanabe, J. Phys. Soc. Jpn. **13**, 880 (1958).

[21] M. H. F. Overwijk, J. I. Dijkhuis, and H. W. de Wijn, Phys. Rev. Lett. **65**, 2015 (1990).